Micro-macro modelling for fluids and powders

Stefan Luding[1,2]

[1] Particle Technology, DelftChemTech, TU Delft, Julianalaan 136, 2628 BL Delft, The Netherlands

[2] e-mail: s.luding@tnw.tudelft.nl

ABSTRACT

One essential question in chemical engineering and material science is, how to bridge the gap between the microscopic picture (kinetic theory or molecular dynamics simulations of fluids or particulate flows) and a macroscopic description on the level of a continuum theory. The former involves impulses/contact-forces and collisions/deformations, whereas the latter concerns tensorial quantities like the stress or the velocity gradient. Applying a consistent averaging formalism, one can obtain scalar- and vector-fields as well as classical tensorial macroscopic quantities like fabric, stress or velocity gradient and, in addition, micropolar quantities like curvature or couple-stress. Generic features in such systems involve enormous inhomogeneities, an-isotropic material behavior, and memory (i.e. history dependence). The stress, strain rate, and structure tensors are, in general, not co-linear, after a small shear deformation. The material acts against shear by gaining stiffness (contacts) as opposed to the compressive shear direction. Numerical and theoretical examples for the micro-macro transition for powders will be given and a generalization to micro- or nano-flows will be discussed.

1 INTRODUCTION

The flow behavior of fluids and powders under large deformations can be studied, using molecular dynamics (MD), also called discrete element method (DEM), a convenient tool to gain insight into the microscopic evolution of, e.g., shear localization. Fluids can be assumed homogeneous on the macroscopic level, but in small geometries (nano- or micro-geometries) or in the presence of macro-molecules or particles, homogeneity can not be taken for granted. Powders are typically inhomogeneous, non-linear, disordered, and an-isotropic on a "microscopic" scale, where the typical microscopic size is the particle size, but those effects can extent up to the macroscopic level, see [1-3] for recent literature.

Thus, since fluids in micro- or nano-geometries and powders can show similar phenomenology, we continue with powders as example for the micro-macro transition approach. An inhomogeneous, random powder responds to deformations via irregular and anisotropic rearrangements and a peculiar stress-response. An initially isotropic contact network becomes anisotropic before the structure of the network reaches its limit of stability, i.e., the yield stress. Before the peak, one has softening, and beyond weakening is obtained [2-5], which is typical for over-consolidated powders. Our work complements recent studies on shear band formation in frictional-cohesive granular media [4-8], for micro- and macro-modeling [9,10], and in various systems [11-14] for different materials.

Besides spheres, non-spherical particles like polygons can also be used [5], or roughness can be mimicked by additional torques [15]. The recently developed micro-macro transition procedures [6-13] aim at a better understand of the macroscopic fluid/powder flow behavior on microscopic foundations. Besides the experimental verification of the simulation results [14], the formulation of constitutive relations in the framework of continuum theory is the great challenge. One promising

material model for sand is the hypoplastic theory [16-20], for which the material parameters can be determined experimentally, or from DEM simulations, as shown in this study.

2 MODEL

2.1 Simulation Details

The elementary units of powders are ”mesoscopic” grains that locally, at the contact point, deform under stress. Since the realistic modeling of the deformations inside the particles is much too complicated, the interaction force is related to the overlap Δ of two particles in contacts, see Fig. 1. Two particles interact only if they are in contact, so that long range forces like electrostatic or van-der-Waals interactions are neglected here. The contact force between two particles is decomposed into a normal and a tangential part and, for the sake of simplicity, we restrict ourselves to spherical particles here. The normal force is, in the simplest case, a linear spring that takes care of repulsion, and a linear dashpot that accounts for dissipation during contact. The tangential force involves dissipation due to Coulomb friction, but also some tangential elasticity that allows for stick-slip behavior on the contact level [4,9,10,13,14].

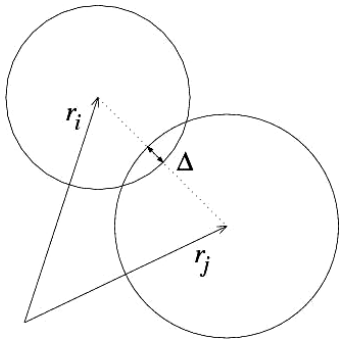

Figure 1: Two particle contact with overlap Δ.

If all forces acting on a selected spherical particle (either from other particles, from boundaries or from external forces) are known, the problem is reduced to the integration of Newton's equations of motion for the translational and rotational degrees of freedom:

$$m_i \frac{\mathrm{d}^2}{\mathrm{d}t^2}\mathbf{r}_i = \mathbf{f}_i + m_i\mathbf{g} \quad \text{and} \quad I_i \frac{\mathrm{d}}{\mathrm{d}t}\boldsymbol{\omega}_i = \mathbf{t}_i \ , \tag{1}$$

with the gravitational acceleration $\mathbf{g}$, mass m_i of the particle, its position $\mathbf{r}_i$, the total force $\mathbf{f}_i = \sum_c \mathbf{f}_i^c$, acting on it due to contacts with other particles or with the walls, its moment of inertia I_i, its angular velocity $\boldsymbol{\omega}_i$, and the total torque $\mathbf{t}_i = \sum_c \mathbf{l}_i^c \times \mathbf{f}_i^c$, with the center-contact “branch” vector $\mathbf{l}_i^c$.

2.2 Model System

Our simulations with the discrete element model [4-10] use a two-dimensional bi-axial box, see Fig. 2, where the left and bottom walls are fixed. Stress- or strain-controlled deformation is applied to the side- and top-walls, respectively. In a typical simulation, the top wall is slowly shifted downwards, while the right wall moves, controlled by a constant stress p_x, responding on the forces exerted on it by the material in the box. The strain on the top-wall, $\varepsilon_{zz} = 1 - z(t)/z_0$, follows a cosine function, $z(t) = z_f + \frac{1}{2}\left(z_0 - z_f\right)\left(1 + \cos(\omega t)\right)$, for half a period, in order to allow for a smooth start-up

and finish of the motion so that shocks and inertia effects are reduced. Note that the shape of the function is arbitrary as long as it is smooth.

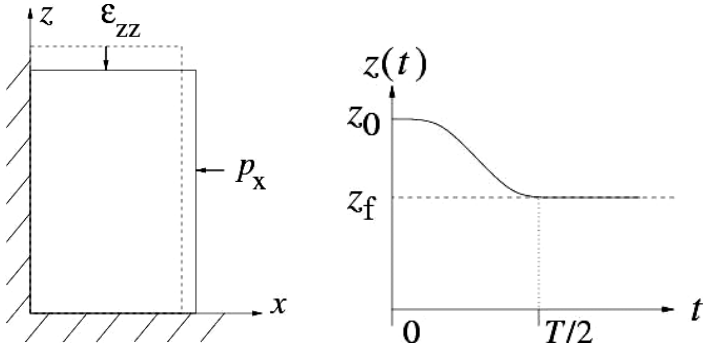

Figure 2: (Left) Schematic drawing of the model system. (Right) Position of the top-wall as function of time for the strain-controlled situation.

2.3 Initial and boundary conditions

Initially, frictionless particles are randomly distributed in a huge box, with rather low overall density. Then the box is compressed by defining an external pressure *p*, in order to achieve a dense, isotropic initial condition. Starting from this relaxed, almost isotropic configuration, the strain ε_{zz} is applied to the top wall and the response of the system is examined, when friction is now active. In terms of a continuum theoretical formulation, the (incremental) stress-strain relation for such a type of simulations can be formulated as tensorial relation

$$\delta\sigma_{ab} = C_{abcd}\varepsilon_{cd} + \delta\sigma_{ab}^{struct.} \quad , \tag{2}$$

with the two known boundary conditions for ε_{zz} and $\delta\sigma_{xx} = 0$, and the two unknowns ε_{xx} and $\delta\sigma_{zz}$. In the following, we will focus on the first term in Eq. (2), the elastic, *reversible* anisotropic stress response, while the second term typically contains the *irreversible* stress changes due to, e.g., reorganization or restructuring of the packing.

Note the non-standard boundary condition that contains unknowns on both left and right hand side. The advantage is that isotropic and deviatoric stress/strain relations are active at the same time, even though this makes the interpretation of the results somewhat more difficult. However, the second advantage of the bi-axial set-up is the fact that the orientation of the eigen-systems of all tensors initially are – and remain – very close to the orientation of the walls (if the walls are smooth).

3 RESULTS

The system examined in the following contains *N*=1950 particles with radii randomly drawn from a homogeneous distribution with minimum 0.5 mm and maximum 1.5 mm. The friction coefficient used in these simulations is μ=0.5.

3.1 Volume- and stress-strain measurements

In Fig. 3 (left), the volume change, $\varepsilon_V = -\Delta V/V_0 = -(\varepsilon_{xx} + \varepsilon_{zz}) - \varepsilon_{xx}\varepsilon_{zz}$, of a typical simulation shows first compression, then dilatancy and, eventually, a very weak change at large deformations, up to 15 per-cent, in the critical flow regime. We note that the maximal compression is reached at deformations increasing with confining stress, but the compression rate is almost independent of the confining stress.

At the same time, the stress response, in Fig. 3 (right) (where the indices *xx* and *zz* denote horizontal and vertical stresses, respectively), shows elastic, softening, and critical state flow behavior. First, the vertical stress increases linearly; then the slope gradually decreases (softening), until the stress reaches its maximum (peak yield stress) in the dilatant regime. After the peak, further softening/weakening behavior (with negative slope) is followed by a constant, strongly fluctuating stress for larger deformations.

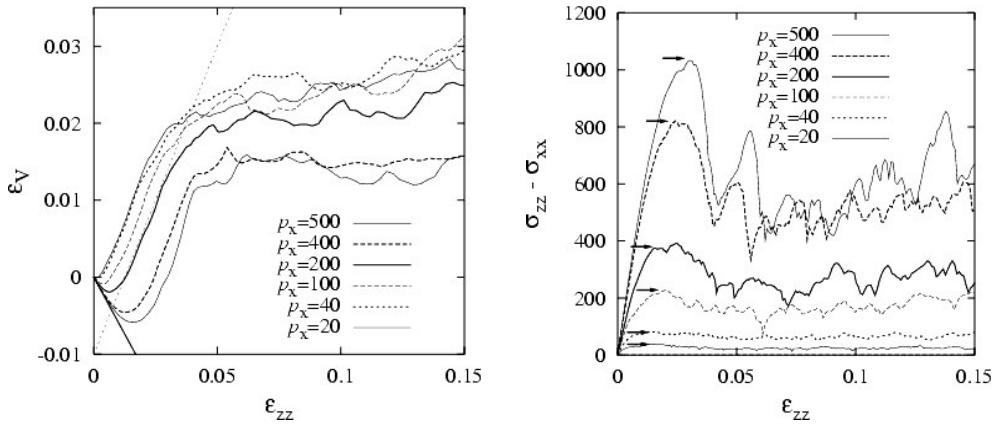

Figure 3: Volumetric strain (left) and stresses (right) during large deformations, both plotted against vertical strain, for different side pressure, as indicated in the inset. The peak yield stresses are marked by arrows.

3.2 Macroscopic material parameters

From the simulation data presented in Fig.3, it is possible to obtain the following material parameters, as based on an isotropy assumption:

(i) The initial slope (-0.59) of the volumetric strain allows to determine the Poisson ratios equivalent for our boundary conditions.

(ii) The slope of the volumetric strain in the dilatancy regime (0.80) is related to the dilatancy angle. Note that it is only weakly dependent on the confining stress for the data presented here, but for larger stresses, the dilatancy angle increases, i.e., the dilatancy occurs more abrupt during smaller vertical deformations.

(iii) The initial slope of the stress is related to the material moduli (data not shown here) and the complete set of material properties can be extracted directly from the simulations [10].

(iv) The peak (yield) stress is related to the flow function of the material, as discussed in detail in the next subsection.

3.3 Peak stress flow function

It is possible to examine the flow behavior of the system by plotting Mohr-circles for the maximum stress (right-most points on the circle) for different confining stresses (left-most points), see Fig. 4. (The eigen-directions of the system are parallel to the walls, because there is no friction active between particles and walls, so that the left- and right-most points on the circles are indeed corresponding to the wall stresses; note that in an arbitrary geometry, it is not necessarily that simple.) The tangent to the circles (slope 0.588) can be seen as the flow function for peak stress. It is linear for the examined parameters, with its slope only slightly larger than expected from the microscopic friction at the contacts alone. Since we have not used cohesive forces, the macroscopic cohesion *c* is non-existent, i.e., the flow function hits the origin. Note that the Mohr circles are obtained in the slow deformation regime, which is not yet strictly the quasi-static regime, i.e., there

is a slightly different outcome if the strain is applied slower. On the other hand, if the strain is applied (much) faster, viscous effects become eminent, especially for the smaller confining stresses, and the results differ a lot from the quasi-static limit. In the quasi-static limit, the slope in Fig. 4 decays to values 0.52-0.54.

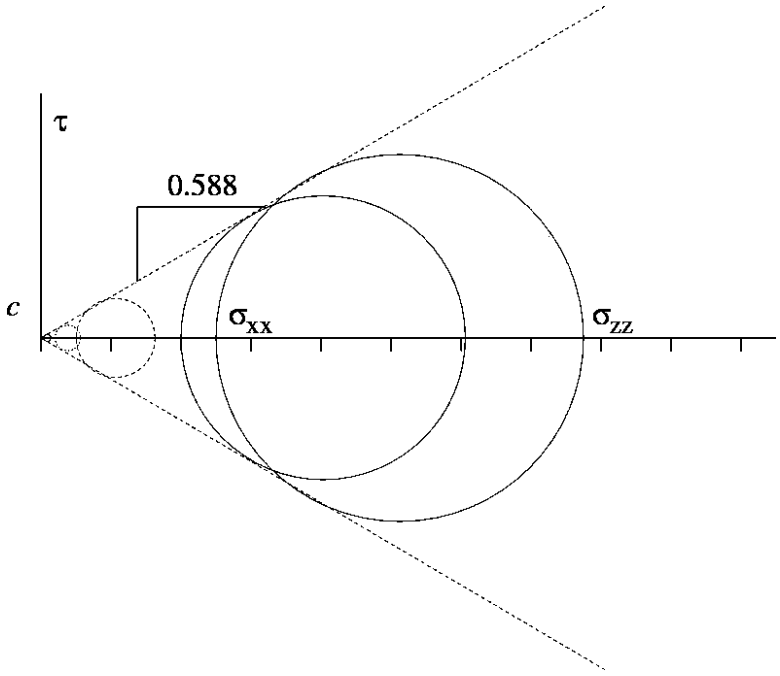

Figure 4: Mohr circle representation of the flow function at peak stress, see the arrows in Fig. 3.

3.4 Some material parameters for Hypoplasticity

Some of the material parameters involved in a hypoplastic material theory [16-20] can also be extracted from the simulation data. An essential ingredient of the theory is the functional behavior of the void ratio:

$$e^h = e_0^h \exp\left(-\left[p/h_s\right]^n\right) , \tag{3}$$

as a function of the pressure. The empirical model parameters for this function (based on experimental findings) involve the void ratio at vanishing stress, e_0^h, the so-called granular hardness, h_s, and an empirical power *n*.

The function in Eq. (3) is astonishingly close to the fit-function for the initial and the critical state void ratio envelope, see Fig. 5:

$$e\left(e_0, n\right) = e_0\left(1-\left[p/h_s\right]^n\right) , \tag{4}$$

where the parameters maximal void ratio $e_0^{loose} \approx 0.244$, critical void ratio $e_0^{crit.} \approx 0.222$, minimal void ratio $e_0^{dense} \approx 0.196$ and $n \approx 2/3$ can be read off from the inset, and the granular hardness, $h_s = 0.12\,10^5$, is set to a value considerably smaller than the spring stiffness used in the DEM contact model. The maximal void ratio e_0^{loose} (minimal density) and the critical void ratio $e_0^{crit.}$ are estimated from the maximal and minimal values reached in the critical state flow regime. Eqs. (3) and (4) can be related to each other via a series expansion in the small variable p/h_s, but a more detailed study of the functional behavior of the void ratio is far from the scope of this study. Even though not all parameters of the hypoplastic material model are accessible from the simulations presented here, the

good agreement between void ratio and pressure behavior from the model and from the simulation is a promising first step.

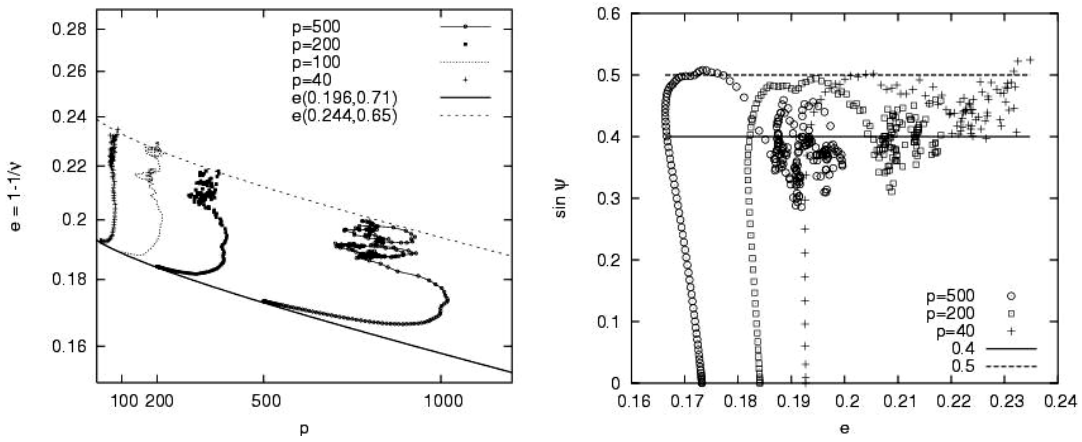

Figure 5: Void ratio, $e=1/\nu-1$, plotted against averaged pressure (left), and deviatoric stress ratio plotted against void ratio (right) – for different confining stresses.

The representation of the deviatoric stress ratio

$$\sin\psi = \frac{\sigma_{zz}-\sigma_{xx}}{\sigma_{zz}+\sigma_{xx}} \ , \tag{5}$$

in Fig. 5 (right) is another way to extract the macroscopic friction angle. For peak stress, the simulation values of $\sin\psi$ are almost in agreement with the microscopic friction coefficient μ=0.5. For critical flow (besides strong scatter due to fluctuations), the macroscopic friction (deviatoric stress ratio) slightly decreases with increasing confining stress. For the largest confining stresses used here, values between 0.3 and 0.45 are realized, whereas for the smaller confining stress, larger values are obtained.

4 SUMMARY AND CONCLUSIONS

In summary, a set of DEM simulations was presented, and several macroscopic material parameters like, e.g., the granular hardness, minimal and maximal void ratios, and a friction angle (deviatoric stress ratio) were extracted from the data. Also the behavior of density (void ratio) and friction angle as function of the confining stress were discussed and related to a hypoplastic material law [16-20]. The present results are a first step towards a micro-macro modeling for frictional powders. Further material parameters have to be identified, and also the effect of cohesion has to be examined more closely, not only for frictionless 2D [11-13], but also for realistic frictional, cohesive 3D materials. The role of particle rotations, as related to micro-polar constitutive models, was not discussed here. In both simulation and experiment, rotations are activated in the shear band – like in micro-polar hypoplastic material models, where the rotational degree of freedom is activated in the shear band too [16-20]. A corresponding parameter identification and the micro-macro-transition is another task for the future, like the implementation and simulation in three-dimensional systems.

Given the fact that a micro-macro transition works for granular materials, as it works for simple fluids, a challenge for the future is to apply the methods presented here to fluid flows in micro- or nano-geometries, where not only anisotropy, but also wall effects like slip at the boundaries or wall

roughness become important. The final goal is to obtain constitutive relations based on microscipic knowledge of the flow behavior.

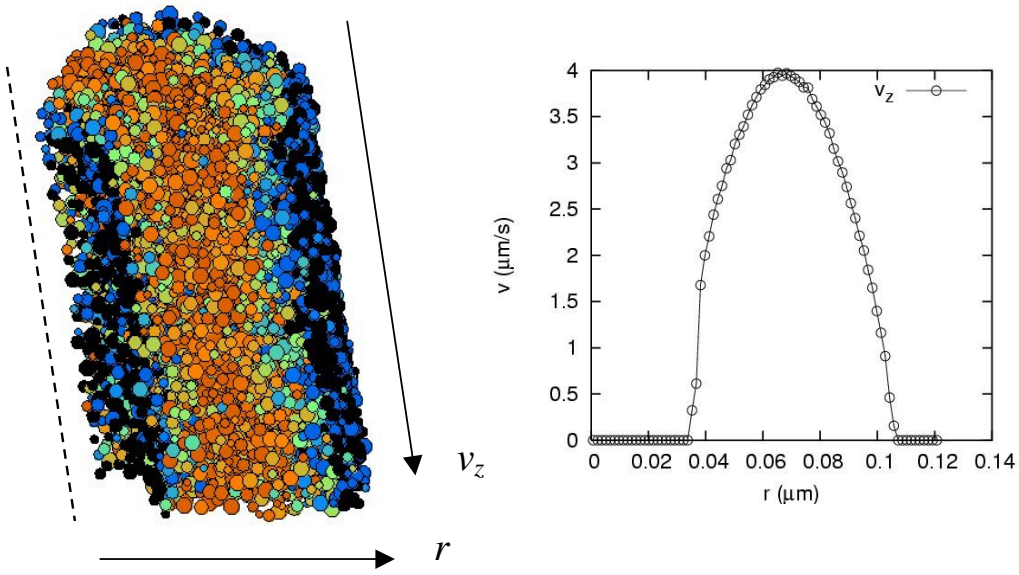

Figure 6: (Left) Snapshot of a MD simulation (with about 10500 particles of size around 3nm) of a micro-flow in a ring-channel; a quarter of the system is shown and the symmetry axis is indicated by the dashed line; radial outward and flow direction are indicated by arrows. The colors denote slow particles (black and blue) close to the wall and fast particles (red) in the center of the channel. (Right) Velocity along the channel as function of the radial distance from the symmetry axis. Besides a parabolic shape in the center of the channel, we note the different wall slip; the wall slip is larger in the inner wall due to its larger curvature.

In Figure 6, an example of a micro flow in a ring channel is presented, where especially the wall slip due to different wall curvature can be observed. Further work in this direction is in progress.

ACKNOWLEDGEMENTS

This work was funded by the Deutsche Forschungsgemeinschaft (DFG) in the framework of the research-group: “Verhalten Granularer Medien”; we acknowledge helpful and inspiring discussions with H.-J. Butt, M. Kappl, M.-K. Müller, K. Nübel, R. Pitchumani, J. Tejchman, J. Tomas, and R. Tykhoniuk.

REFERENCES

[1] H. J. Herrmann, J.-P. Hovi, and S.Luding, eds., *Physics of dry granular media*, NATO ASI Series E 350, Kluwer Academic Publishers, Dordrecht, 1998.

[2] P. A. Vermeer, S. Diebels, W. Ehlers, H. J. Herrmann, S. Luding, and E. Ramm, eds., *Continuous and Discontinuous Modelling of Cohesive Frictional Materials*, Lecture Notes in Physics 568, Springer, Berlin, 2001.

[3] Y. Kishino, ed., *Powders & Grains 2001*, Balkema, Rotterdam, 2001.

[4] C. Thornton and S. J. Antony, Quasi-static deformation of a soft particle system, Powder Technology 109(1-3), 179—191, 2000.
[5] G. A. D'Addetta, F. Kun, E. Ramm, *On the application of a discrete model to the fracture process of cohesive granular materials*, Granular Matter 4 (2), 77-90 2002.
[6] M. Oda and K. Iwashita, *Study on couple stress and shear band development in granular media based on numerical simulation analyses*, Int. J. of Enginering Science 38, 1713-1740, 2000.
[7] N. P. Kruyt and L. Rothenburg, *Statistics of the elastic behavior of granular materials*. Int. J. of Solids and Structures 38, 4879—4899, 2001.
[8] S. Luding, M. Lätzel, W. Volk, S. Diebels, and H. J. Herrmann, *From discrete element simulations to a continuum model*, Comp. Meth. Appl. Mech. Engng. 191, 21-28, 2001.
[9] J. Tomas, *Assessment of mechanical proper-ties of cohesive particulate solids – part 1: particle contact constitutive model*, Particulate Sci. Technol. 19, 95-110, 2001; J. Tomas, *Assessment of mechanical properties of cohesive particulate solids – part 2: powder flow criteria*, Particulate Sci. Technol. 19, 111-129, 2001.
[10] S. Luding, *Micro-macro transition for an-isotropic, frictional granular packings,* Int. J. Sol. Struct. 41(21), 5821-5836, 2004; S. Luding, *Micro-Macro Models for Anisotropic Granular Media*, in: Modelling of Cohesive-Frictional Materials, P. A. Vermeer, W. Ehlers, H. J. Herrmann, E. Ramm (eds.), A. A. Balkema, Leiden, 2004 (ISBN 04 1536 023 4), pp. 195-206.
[11] R. Tykhoniuk, S. Luding and J. Tomas, *Simulation der Scherdynamik von kohäsiven Pulvern*, Chem. Ing. Techn. 76, 59-62, 2004.
[12] S. Luding and H. J. Herrmann, *Micro-Macro Transition for Cohesive Granular Media* ,in: Zur Beschreibung komplexen Materialverhaltens, Institut für Mechanik, S. Diebels (Ed.), Stuttgart, 121--134, 2001.
[13] S. Luding, R. Tykhoniuk, and Jürgen Tomas, *Anisotropic material behavior in dense, cohesive powders*, Chem. Eng. Tech 26 (12), 1229-1232, 2003.
[14] M. Lätzel, S. Luding, H. J. Herrmann, D. W. Howell, and R. P. Behringer, *Comparing Simulation and Experiment of a 2D Granular Couette Shear Device,* Eur. Phys. J. E 11, 325-333, 2003.
[15] M. Oda, *Micro-fabric and couple stress in shear bands of granular materials*, in: Powders and Grains, C. Thornton, ed., Rotterdam, Balkema, 161-167, 1993.
[16] J. Tejchman and W. Wu, *Numerical study on patterning of shear bands in a Cosserat continuum*, Acta Mechanica 99: 61-74,1993.
[17] E. Bauer and W. Huang, *Numerical study of polar effects in shear zones*, in: Numerical Models in Geomechanics, G.N. Pande, S. Pietruszczak, H. F. Schweiger, eds., Balkema, 133-141, 1999.
[18] E. Bauer, *Calibration of a comprehensive hypoplastic model for granular materials,* Soils and Foundations 36, 13-26, 1996.
[19] J. Tejchman, *Patterns of shear zones in granular materials within a polar hypoplastic continuum*, Acta Mechanica 155, 71-95, 2002.
[20] K. Nübel, *Experimental and Numerical Investigation of shear localization in granular material*, PhD thesis, Karlsruhe, 2002.